Journal of Alloys and Compounds 708 (2017) 827–833

Contents lists available at ScienceDirect

Journal of Alloys and Compounds

journal homepage: http://www.elsevier.com/locate/jalcom

Observation and photoluminescence properties of two Er^{3+} centers in $CaSc_2O_4$:Er^{3+}, Yb^{3+} upconverting phosphor

Leyu Feng [a, b], Zhendong Hao [a, *], Yongshi Luo [a], Xia Zhang [a], Liangliang Zhang [a], Guohui Pan [a], Huajun Wu [a], Jiahua Zhang [a, **]

[a] State Key Laboratory of Luminescence and Applications, Changchun Institute of Optics, Fine Mechanics and Physics, Chinese Academy of Sciences, 3888 Eastern South Lake Road, Changchun, 130033, China
[b] Graduate School of Chinese Academy of Sciences, Beijing 100039, China

ARTICLE INFO

Article history:
Received 6 December 2016
Received in revised form
6 March 2017
Accepted 9 March 2017
Available online 9 March 2017

Keywords:
Upconversion
Energy transfer
Two Er^{3+} centers

ABSTRACT

$CaSc_2O_4$ phosphors codoped with 0.2% Er^{3+} and various concentrations (0–15%) of Yb^{3+} are prepared by high temperature solid-state reaction. Two Er^{3+} luminescence centers are observed and they are assigned to substitution for Ca^{2+} site (Er^{3+}(I)) and Sc^{3+} site (Er^{3+}(II)), respectively. We find that the Er^{3+}(I) centers are preferentially formed at low doping concentration and their number starts to decrease along with the increase of the Er^{3+}(II) centers on increasing Yb^{3+} concentration. Meanwhile, intense upconversion luminescence (UCL) with color tuning from green to red is observed upon 980 nm excitation. The decomposition of the UCL spectra exhibits the main contribution from the Er^{3+}(I) centers in the range of Yb^{3+} concentration of this work. This result is attributed to efficient emissions of the Er^{3+}(I) centers for the long lifetimes of Er^{3+}(I) both on the green and red emitting levels. Furthermore, we have observed the UCL intensity of $CaSc_2O_4$: 0.2% Er^{3+}, 15% Yb^{3+} is 4 times as strong as that in Y_2O_3: 0.2 Er^{3+}, 15% Yb^{3+}.

1. Introduction

Infrared to visible upconversion luminescence in rare earth ions doped materials have been extensively studied for its fundamental value and its potential applications in biological imaging, visible lasers, optical communication and so on [1–4]. Among the rare earth ions, Er^{3+}/Yb^{3+} combination is the most attractive system for energy transfer up-conversion, which contains a red emission around 670 nm and a green emission around 560 nm originated from $^4F_{9/2} \rightarrow {}^4I_{15/2}$ and $^2H_{11/2}$, $^4S_{3/2} \rightarrow {}^4I_{15/2}$ of Er^{3+}, respectively [5]. This combination is beneficial for biological imaging owing to the red emission band of Er^{3+} centered around 670 nm well matching the optical transparent window (650–1100 nm) of biological tissues. In consequence, it is significant to achieve a strong red to the green emission intensity ratio (R/G). At present, the Er^{3+}/Yb^{3+} codoped $NaYF_4$ is one of the most efficient upconversion materials [6,7]. However, the emission usually presents intense green UCL, which hinders their application in UC bioimaging. On the other hand, poor physical and chemical stability also limited the application of $NaYF_4$ [8]. Oxide UC materials become attractive for the considerable chemical durability and thermal stability. Therefore, it is expected to achieve highly efficient red UCL in Er^{3+}/Yb^{3+} co-doped oxide system.

$CaSc_2O_4$ is a promising oxide host for efficient UCL due to low phonon energy of about 540 cm^{-1}, which is lower than Y_2O_3 (phonon energy of 600 cm^{-1}) [9]. Intense visible UCL was obtained in $CaSc_2O_4$ codoped with Ho^{3+} and Yb^{3+} [10,11], Tm^{3+} and Yb^{3+} [9,12,13], and with Er^{3+} and Yb^{3+} [14,15]. It is noteworthy that R/G in $CaSc_2O_4$: Er^{3+}/Yb^{3+} is higher than that in $NaYF_4$. As we have known, the structure of $CaSc_2O_4$ has an orthorhombic $CaFe_2O_4$ structure with a space group Pnam. In this structure, Ca^{2+} ions occupy an 8-fold coordinated position and Sc^{3+} ions occupy two 6-fold coordinated positions [16]. The ionic radius of Sc^{3+} is 0.745 Å, while the ionic radius of Ca^{2+} is 1.12 Å. Considering both Er^{3+} (r = 0.945 Å for CN = 8, r = 0.890 Å for CN = 6) and Yb^{3+} (r = 0.985 Å for CN = 8, r = 0.868 Å for CN = 6) ions are smaller than Ca^{2+} and bigger than Sc^{3+} [17], which could enter Sc^{3+} and Ca^{2+} positions simultaneously. However, the two kinds of Er^{3+} UCL have not been reported. If we can distinguish the UC efficiency of

* Corresponding author.
** Corresponding author.
E-mail addresses: haozd@ciomp.ac.cn (Z. Hao), zhangjh@ciomp.ac.cn (J. Zhang).

http://dx.doi.org/10.1016/j.jallcom.2017.03.088
0925-8388/

Er^{3+} ions at different sites, it will provide a new way to improve the R/G.

In this paper, it is first time to report two Er^{3+} centers photoluminescence (PL) and UCL properties in $CaSc_2O_4$. We found that Er^{3+} at Ca^{2+} site (Er^{3+}(I)) make the main contribution to the UCL, that is attributed to longer fluorescence lifetimes than Er^{3+} at Sc^{3+} site (Er^{3+}(II)). Furthermore, the intense UCL was observed in Er^{3+} and Yb^{3+} codoped $CaSc_2O_4$ compared with Y_2O_3: Er^{3+}, Yb^{3+}.

2. Experimental

The $CaSc_2O_4$: 0.2% Er^{3+}, xYb^{3+} (x = 0%, 2%, 5%, 10% and 15%) powder samples were synthesized by high temperature solid state reaction [18]. The initial content of Yb^{3+} and Er^{3+} are calculated according to substitution for Sc^{3+} site, which can be expressed by the formula $CaSc_{2-0.002-x}Er_{0.002}Yb_xO_4$. The starting materials were high purity $CaCO_3$, Sc_2O_3, Er_2O_3 and Yb_2O_3. After a good mixing in an agate mortar with stoichiometric molar ratios, the powers were placed in a crucible with a lid, then sintered at 1500 °C for 4 h. The doped $Y_{2-0.002-0.15}Er_{0.002}Yb_{0.15}O_3$ powder for comparing with $CaSc_2O_4$ was prepared by firing precursors methods that have intense UCL than solid state reaction. Starting aqueous solutions $Y(NO_3)_3$, $Yb(NO_3)_3$ and $Er(NO_3)_3$ with corresponding mole ratios were mixed and stirred vigorously to form a homogeneous solution. The sample was obtained after being dried at 100 °C for 12 h and then pre-fired at 800 °C for 4 h, finally, sintered at 1600 °C for 6 h after following the intermediate grinding. Both Er^{3+} and Yb^{3+} are space homogeneous distribution for the equal probability on occupying site of the host lattice.

The phase purity and crystal structure of the powder samples were examined by X-ray diffraction (XRD) in a Bruker D8-Focus automatic diffractometer with Cu Kα1 radiation (λ = 0.15406 nm). Step scans were performed from 20° to 75° 2θ and step size of 0.02° with a count time of 0.1 s/step. The PL, photoluminescence excitation (PLE) and UCL spectra were measured using an EI-FS920 spectrometer with a xenon lamp as the excitation source for PL and PLE. A CW 980 nm laser diode with 330 mV was used as the excitation source for UCL. In fluorescence lifetime measurements, an optical parametric oscillator (OPO) was used as an excitation source, and the signals were detected by a Tektronix digital oscilloscope (TDS 3052).

3. Results and discussion

The structures characterized by the XRD patterns are shown in Fig. 1(a) for the samples with nominal compositions of $CaSc_2O_4$:0.2% Er^{3+}, xYb^{3+} (x = 0%, 2%, 5%, 10%, 15%). It is obvious that all the diffraction peaks of the samples are matched well with the reported $CaSc_2O_4$ phase (JCPDS#20-0234), indicating the successful preparation of $CaSc_2O_4$ phase. The structure of $CaSc_2O_4$ has an orthorhombic $CaFe_2O_4$ structure with space group Pnam (No.62) and lattice constants a ≠ b ≠ c, α = β = γ = 90°, as is shown in Fig. 1(b). In this structure, Ca^{2+} is 8-fold and Sc^{3+} is 6-fold. $CaSc_2O_4$ contains two crystallographic Sc^{3+} sites with the similar average distance for Sc–O bond (2.1206 Å and 2.1226 Å).

Fig. 2 shows the PL spectra of $CaSc_2O_4$: 0.2% Er^{3+}, xYb^{3+} upon Er^{3+} $^4F_{7/2}$ excitation at 492 nm. The characteristic emissions of Er^{3+} appear in the green (510–580 nm) and red (640–700 nm) spectral regions, which are originated from $^2H_{11/2}$, $^4S_{3/2} \rightarrow {}^4I_{15/2}$ and $^4F_{9/2} \rightarrow {}^4I_{15/2}$ transitions of Er^{3+}, respectively. It is noticed that the red emission intensities grow up relative to the green emissions with increasing concentration of Yb^{3+}. This is attributed to the CRB processes for populating Er^{3+} $^4F_{9/2}$ [19], described as deexcitation from Er^{3+} $^4S_{3/2}$ to Er^{3+} $^4I_{13/2}$ by transferring energy to Yb^{3+}, followed by energy back transfer from the excited Yb^{3+} to the same Er^{3+} to promote the excitation from Er^{3+} $^4I_{13/2}$ to Er^{3+} $^4F_{9/2}$, as shown in Fig. 3. More importantly, it is found that the spectral distribution of the green emission changes with Yb^{3+} concentration. It is clear that the peak at 544 nm decreases and the peaks at 557 nm and 565 nm enhance relative to the main peak with the increase of Yb^{3+} concentration. It should be noted that the same behavior is also observed in Er^{3+} singly doped $CaSc_2O_4$ when Er^{3+} concentration is continuously increased. Considering the emission shape of Er^{3+} is mainly due to its local structure and the coordination number [20]. Therefore, the results indicate that there are two distinct distinguishable Er^{3+} centers and the number ratio of them varies with the dopants concentration. Here, the peak at 544 nm is assigned to one Er^{3+} center labeled as Er^{3+}(I), and the peaks at 557 nm and 565 nm are assigned to the same Er^{3+} center labeled as Er^{3+}(II).

In order to achieve the individual PL spectrum of the two Er^{3+} centers, the PLE spectra of $CaSc_2O_4$: 0.2% Er^{3+}, 10% Yb^{3+} monitored at 544 nm of Er^{3+}(I) and 565 nm of Er^{3+}(II) are measured and displayed together in Fig. 4. The PLE spectra of the two centers are indeed difference, being helpful to determine the preferential excitation wavelength for each center. To obtain the PL spectrum of Er^{3+}(I), we select the Yb^{3+} free sample $CaSc_2O_4$: 0.2% Er^{3+} because Er^{3+}(I) dominates the spectrum in this sample (see Fig. 2). Similarly, we select highly Yb^{3+} doped sample $CaSc_2O_4$: 0.2% Er^{3+}, 15% Yb^{3+} to obtain the PL spectrum of Er^{3+}(II) because the emissions of Er^{3+}(II) enhance rapidly on increasing Yb^{3+} concentration (see Fig. 2). Finally, the spectra of the green and red emissions of the two Er^{3+} centers are obtained individually using the excitation wavelength of 487 nm for Er^{3+}(I) and of 488.2 nm for Er^{3+}(II). Accordingly, the PL spectra in Fig. 2 are decomposed into Er^{3+}(I) and Er^{3+}(II), as shown in Fig. 5. The emission spectra of the two centers are considerably different. For instance, Er^{3+}(I) appears a characteristic green emission line at 544 nm and Er^{3+}(II) appears one at 565 nm with a red emission peak at 683 nm.

In Fig. 5, the emissions of Er^{3+}(I) in the green region decreased with the increase of Yb^{3+}, while the emissions of Er^{3+}(II) in the same region enhanced with the increasing Yb^{3+} concentration up to 5% and decreases after that. The enhancement of the Er^{3+}(II) in the green emissions means the increase of Er^{3+}(II) centers, and the subsequent reduction of the green emission is attributed to luminescence quenching by Yb^{3+} through the cross-relaxation (CR). The CR is also the main reason for the monotonous decrease of the Er^{3+}(I) in the green region on increasing x, while the reduction of Er^{3+}(I) number is also suggested to be a reason for the intensity reduction of Er^{3+}(I) centers in view of the increase of Er^{3+}(II) centers for a fixed number of the total Er^{3+} ions. The red emissions of the two Er^{3+} centers also show different behaviors in Fig. 5. Emission intensities of Er^{3+}(I) and Er^{3+}(II) are obtained from the integral spectra and showed in Fig. 6. From Fig. 6, the R/G for Er^{3+}(I) is enhanced by a factor of 50.8 with increasing Yb^{3+} concentration from 0 to 15%, but that for Er^{3+}(II) is enhanced by only 2.3. This indicates that Er^{3+}(I) has an more efficient CRB process than Er^{3+}(II). The result is further supported by the observation of an efficient CR process of Er^{3+}(I) based on the fluorescence decay.

Fig. 7 shows the decay curves of the green emission at different Yb^{3+} concentrations after direct excitation of the $^2H_{11/2}$ level at 525 nm for Er^{3+}(I) (a) and at 519 nm for Er^{3+}(II) (b). The two Er^{3+} centers exhibit a single exponential decay in the Yb^{3+} free sample $CaSc_2O_4$: 0.2% Er^{3+}. The $^4S_{3/2}$ lifetime of Er^{3+}(I) appears to be much longer than that of Er^{3+}(II). With the increasing Yb^{3+} concentration, the decays become faster and nonexponential due to the CR. The efficiency (η_{CR}) of the CR can be calculated by

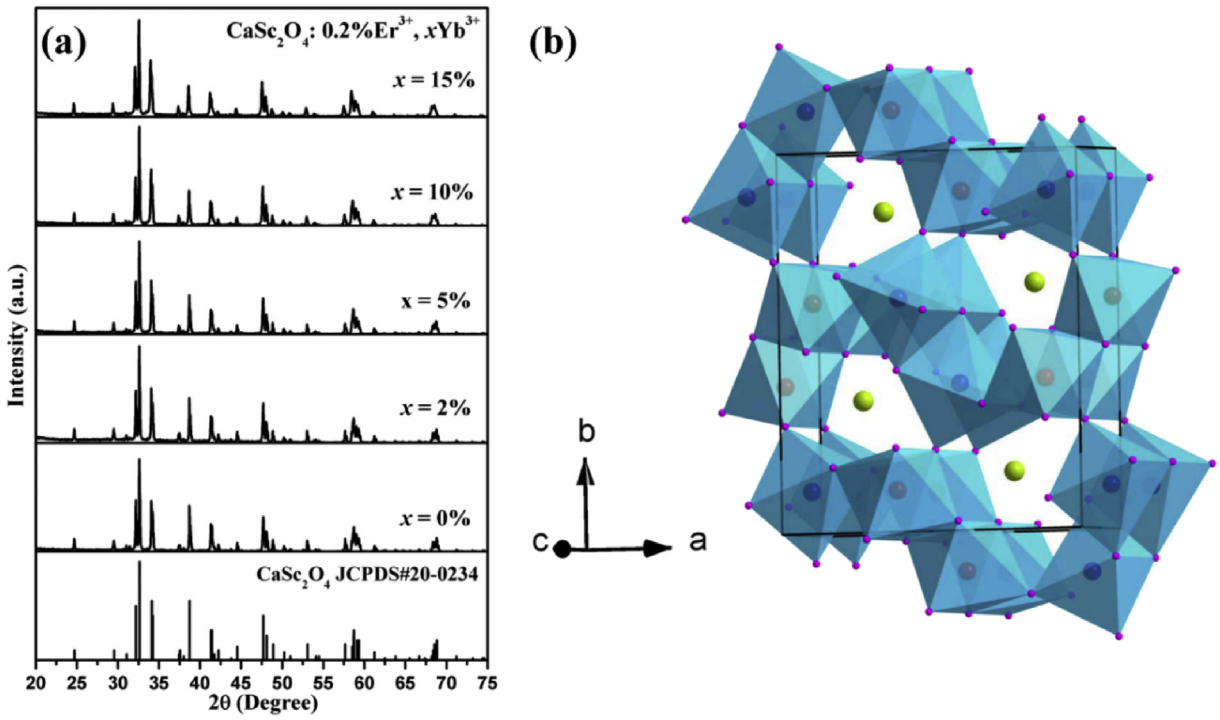

Fig. 1. (a) XRD patterns of $Ca_2Sc_2O_4$: 0.2% Er^{3+}, xYb^{3+}. The standard card (JCPDS#20-0234) for $Ca_2Sc_2O_4$ is also given for comparison; (b) Crystal structure of $CaSc_2O_4$ with coordination configurations of Ca^{2+} (green) and two crystallographic Sc^{3+} sites (red and blue). with the same coordination number of 6 and the similar average Sc-O bond length. (For interpretation of the references to colour in this figure legend, the reader is referred to the web version of this article.)

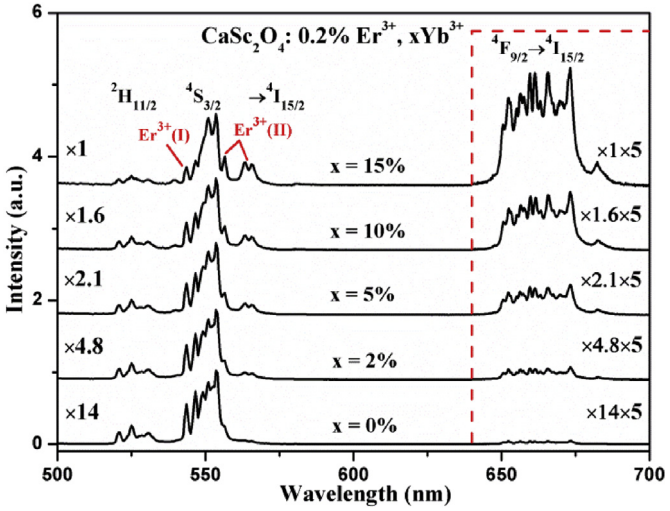

Fig. 2. PL spectra of $CaSc_2O_4$: 0.2% Er^{3+}, xYb^{3+} upon Er^{3+} $^4F_{7/2}$ excitation at 492 nm.

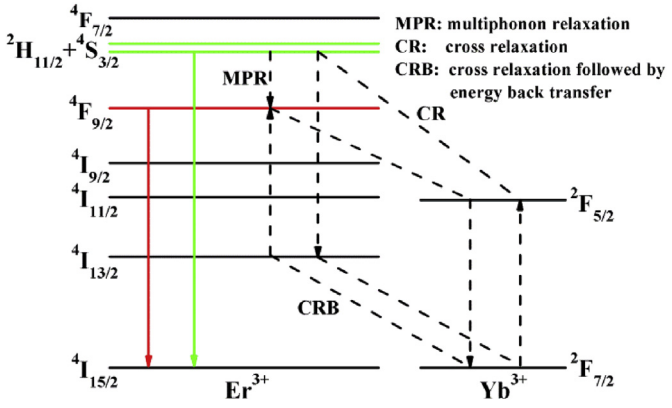

Fig. 3. Energy level diagram illustrating the CRB processes for populating the red emitting level $^4F_{9/2}$ from the green emitting level $^4S_{3/2}$ of Er^{3+}. (For interpretation of the references to colour in this figure legend, the reader is referred to the web version of this article.)

$$\eta_{CR} = 1 - \frac{\tau}{\tau_0} \quad (1)$$

where τ and τ_0 are the $^4S_{3/2}$ lifetimes of Er^{3+} in the presence and absence of Yb^{3+}, respectively. The $^4S_{3/2}$ lifetimes are defined as the area under the decay curves in Fig. 7. The lifetimes and the calculated CR efficiencies using Eq. (1) are listed in Table 1. It is presented that the CR efficiency of Er^{3+}(I) is greater than Er^{3+}(II). Hence, a remarkable increment of the R/G ratio for high Yb^{3+} content in Er^{3+}(I) rather than in Er^{3+}(II) is understandable.

The lifetimes of the red emitting level $^4F_{9/2}$ of the two Er^{3+} centers are also evaluated. Fig. 8 shows the fluorescence decay curves monitored at 665 nm (a) and 683 nm (b) after the $^4F_{9/2}$ states of the two Er^{3+} centers are both excited at 654 nm in $CaSc_2O_4$: 0.2% Er^{3+}, xYb^{3+}. The decay curves contain a slow and a fast component. With the increase of x, the slow component is reduced and the fast one is increased. In the decay patterns monitored at 683 nm, the fast component dominates the decay for high Yb^{3+} content. Furthermore, it is found that Fig. 7(a) and (b) appear the same decay time of the fast process and the slow process for each sample. Accordingly, it is suggested that the decay patterns are the consequences of the combination of the two Er^{3+} centers. Owing to the decrease of Er^{3+}(I) centers and increase of Er^{3+}(II) centers with the increasing x, the slow component and the fast component are attributed to Er^{3+}(I) and Er^{3+}(II), respectively. The monitored

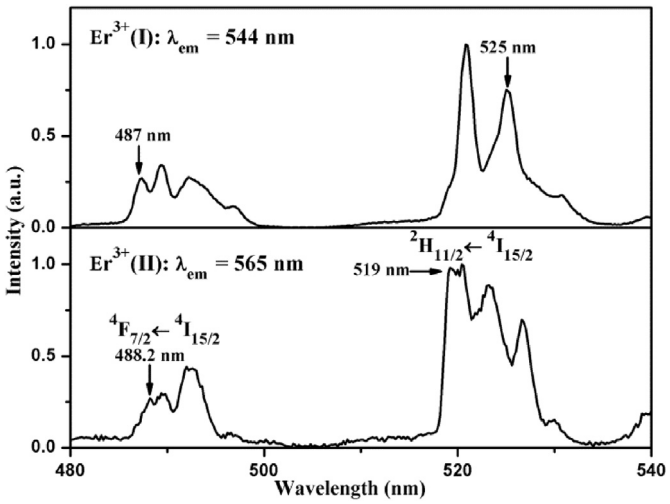

Fig. 4. PLE spectra of $CaSc_2O_4$: 0.2% Er^{3+}, 10% Yb^{3+} monitored at 544 nm of Er^{3+}(I) and 565 nm of Er^{3+}(II).

wavelength of 683 nm is a preferential wavelength for collecting Er^{3+}(II) emission (see Fig. 5). Therefore, the decay patterns in Fig. 8(b) appear more fast components than in Fig. 8(a). It is noticed the decay patterns for monitored at 683 nm are also governed by slow components for low Yb^{3+} content. This is because the number of Er^{3+}(II) centers is much less than that of Er^{3+}(I) centers for low Yb^{3+} content, thus, more photons of Er^{3+}(I) emission are collected.

The decay curves have been well fitted by a biexponential decay function. The obtained $^4S_{3/2}$ and $^4F_{9/2}$ lifetimes of the two centers are listed in Table 1. Compared with the $^4S_{3/2}$ lifetimes, a small shortening of the $^4F_{9/2}$ lifetime on increasing Yb^{3+} concentration is observed. This is due to the weak coupling of Er^{3+} $^4F_{9/2} \rightarrow {}^4I_{15/2}$ with Yb^{3+} $^2F_{7/2} \rightarrow {}^2F_{5/2}$ [21]. One can find the fluorescence lifetime of Er^{3+}(I) is always longer than that of Er^{3+}(II) for both the green and red emissions. For instance, $CaSc_2O_4$: 0.2% Er^{3+} has the $^4F_{9/2}$ lifetime of 64 μs for Er^{3+}(I) much longer than 8 μs for Er^{3+}(II). If the radiative lifetimes of the two centers are similar, it is therefore suggested that the red emission of Er^{3+}(I) is more efficient than that of Er^{3+}(II).

Since number of the Er^{3+}(I) centers decreases and that of the Er^{3+}(II) centers increases with increasing Yb^{3+}, we propose that Er^{3+}(I) and Er^{3+}(II) correspond to substitution for Ca^{2+} and Sc^{3+} sites, respectively. The explanations are as follows: Both Er^{3+} (r = 0.945 Å for CN = 8, r = 0.890 Å for CN = 6) and Yb^{3+} (r = 0.985 Å for CN = 8, r = 0.868 Å for CN = 6) ions are smaller than Ca^{2+} (r = 1.12 Å for CN = 8) and bigger than Sc^{3+} (r = 0.745 Å for CN = 6), it is expected that Er^{3+} and Yb^{3+} ions could preferentially occupy Ca^{2+} site. However, further occupation could be restricted by the charge difference between Er^{3+}, Yb^{3+} ions and Ca^{2+} ions, owing to a low solubility of Er^{3+} and Yb^{3+} ions at Ca^{2+} sites. From this viewpoint, continuously increase Yb^{3+} content could saturate the replacement of Ca^{2+} site and it thus forces more and more Er^{3+} ions to occupy Sc^{3+} site. The crystal structure of $CaSc_2O_4$ contains one Ca^{2+} site and two Sc^{3+} sites to be possibly replaced by Er^{3+} and Yb^{3+} ions. The two Sc^{3+} sites have the same coordination number (CN = 6) and the similar average distance for Sc–O bond (2.1206 Å

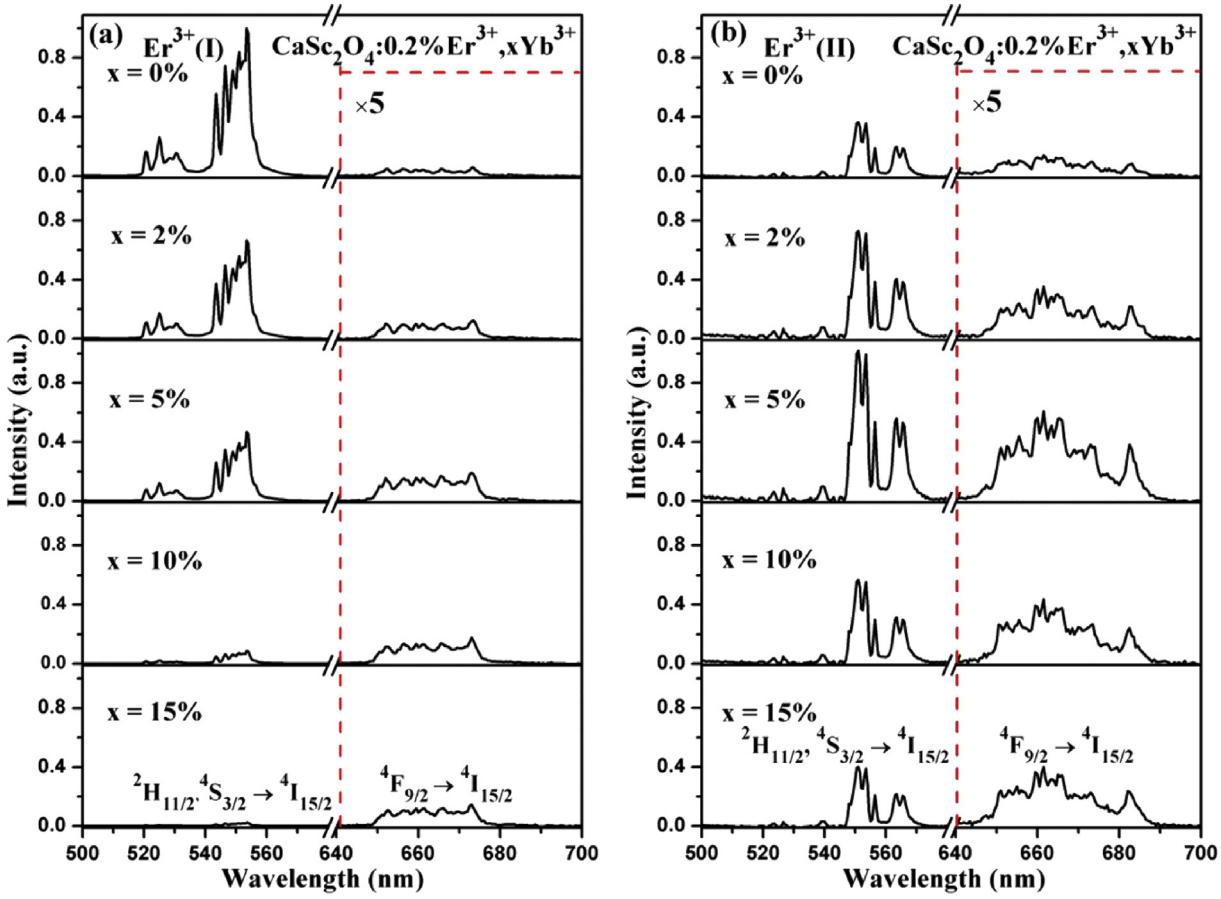

Fig. 5. Emission spectra of Er^{3+}(I) center (a) and Er^{3+}(II) center (b) decomposed from the spectra in Fig. 2 for $CaSc_2O_4$: 0.2% Er^{3+}, xYb^{3+}. The spectra are normalized for each center.

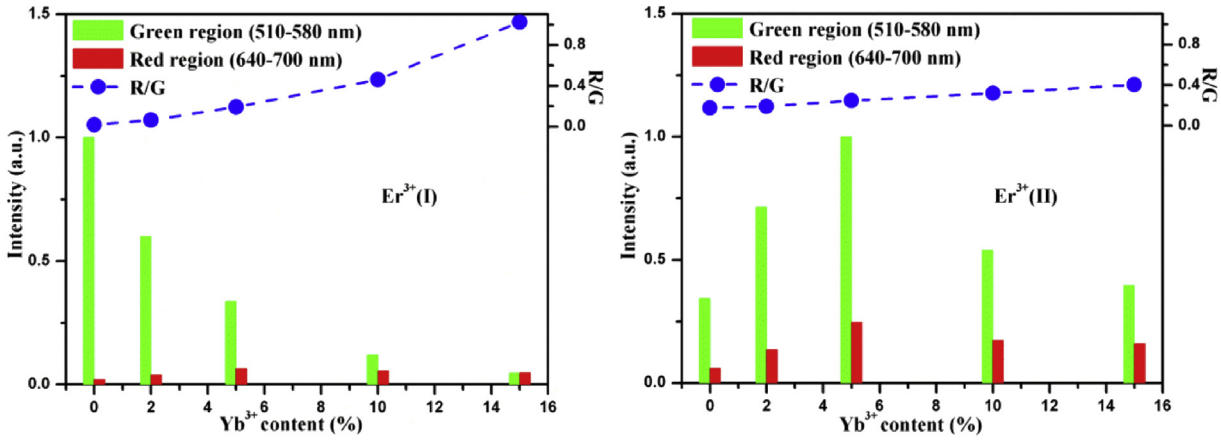

Fig. 6. R/G for Er3+(I) centers (a) and Er3+(II) centers (b) are represented by the right axis. The green bar and the red bar indicate the emission intensity of the green (510–580 nm) spectra region and the red (640–700 nm) spectra region, respectively. (For interpretation of the references to colour in this figure legend, the reader is referred to the web version of this article.)

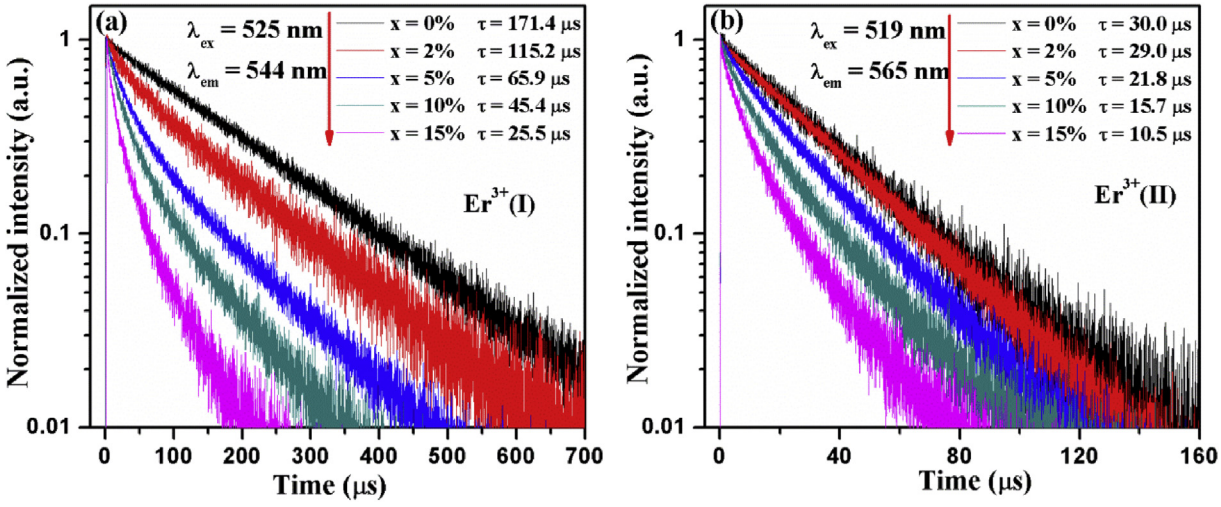

Fig. 7. Green fluorescence decay curves of the Er^{3+}(I) (a) and Er^{3+}(II) (b) in $CaSc_2O_4$: 0.2% Er^{3+}, xYb^{3+}.

Table 1
The fluorescence lifetimes of Er^{3+} and the calculated CR efficiencies for $CaSc_2O_4$: 0.2%Er^{3+}, xYb^{3+}.

x	Green $^4S_{3/2}$				Red $^4F_{9/2}$	
	Er^{3+}(I)		Er^{3+}(II)		Er^{3+}(I)	Er^{3+}(II)
	τ (μs)	η_{CR} (%)	τ (μs)	η_{CR} (%)	τ (μs)	τ (μs)
0	171.4	0	30.0	0	64.0	8.0
0.02	115.2	32.8	29.0	3.1	63.5	7.5
0.05	65.9	61.6	21.8	27.1	58.1	7.0
0.10	45.4	73.5	15.7	47.5	55.0	6.0
0.15	25.5	85.0	10.5	64.9	50.8	5.2

and 2.1226 Å). Thus, Er^{3+} ions on the two Sc^{3+} sites may exhibit spectrally unresolved luminescence using the measurement conditions of this work. Considering the average distance for Ca–O bond (2.4 Å) is much longer than that for Sc–O bond (2.1 Å), the Er^{3+}(I) center at Ca^{2+} site experiences low local phonon vibration with respect to Er^{3+}(II). Accordingly, the Er^{3+}(I) undergoes slower multiphonon relaxation and longer fluorescence lifetime than Er^{3+}(II).

Fig. 9 shows the UCL spectra for $CaSc_2O_4$: 0.2%Er^{3+}, xYb^{3+} (x = 0%, 2%, 5%, 10% and 15%) upon 980 nm excitation. Each spectrum is decomposed into Er^{3+}(I) emission and Er^{3+}(II) emission. It is clearly demonstrated that Er^{3+}(I) governs the UCL for the low concentration of Yb^{3+} and Er^{3+}(II) gradually becomes pronounced with the increase of Yb^{3+} concentration, reflecting the number change of the two centers. At the high doping content of Yb^{3+}, the UCL is dominated by the red emission due to strong CRB processes in energy transfer upconversion [19]. Meanwhile, Er^{3+}(I) still makes the main contribution to the UCL, reflecting the advantage of a long $^4F_{9/2}$ lifetime of Er^{3+}(I). Considering the $^4F_{9/2}$ lifetime (64 μs) is also longer than that (24 μs) of Er^{3+} in Y_2O_3: 0.2%

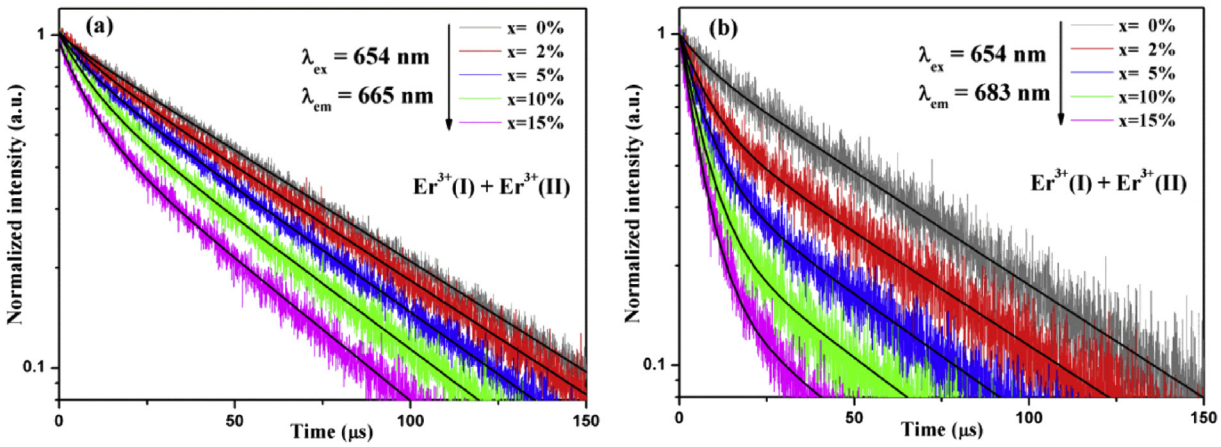

Fig. 8. Red fluorescence decay curves monitored at 665 nm (a) and 683 nm (b) after direct excitation of the $4F_{9/2}$ level at 654 nm in $CaSc_2O_4$: 0.2%Er^{3+}, xYb^{3+}. The fitting data (black solid) given by a biexponential decay function are also presented.

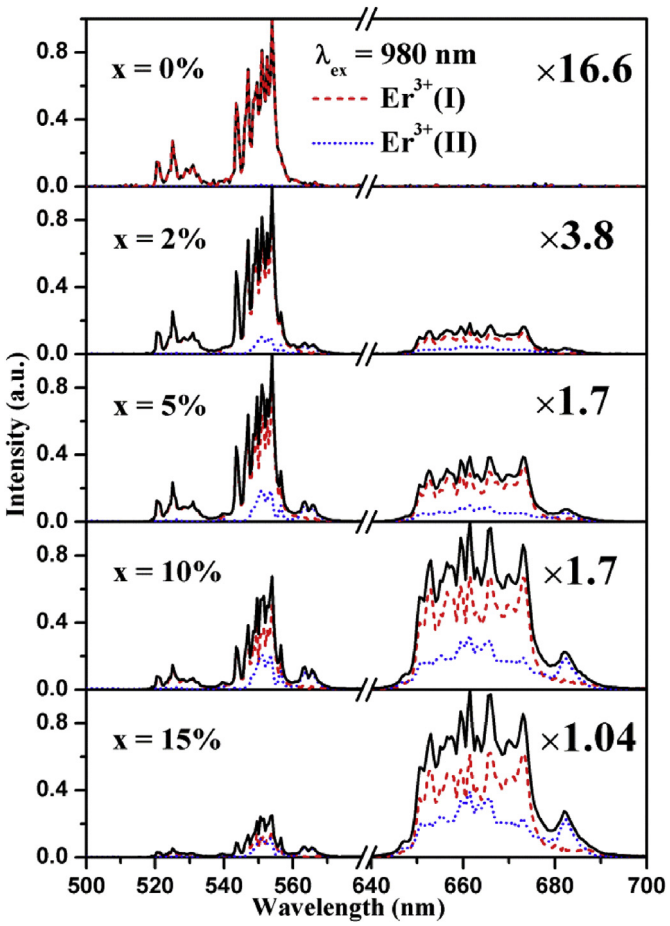

Fig. 9. UCL spectra upon 980 nm excitation for $CaSc_2O_4$: 0.2%Er^{3+}, xYb^{3+}. The individual emission of Er^{3+}(I) (red dashed) and Er^{3+}(II) (blue dotted) are presented. (For interpretation of the references to colour in this figure legend, the reader is referred to the web version of this article.)

Er^{3+} [19], To compare the UCL intensities in the two hosts is a great interest to us.

Fig. 10 shows the UCL spectra of $CaSc_2O_4$: 0.2% Er^{3+}, 15% Yb^{3+} and Y_2O_3: 0.2%Er^{3+}, 15% Yb^{3+} under 980 nm excitation. The same fractional doping concentration for the two hosts corresponds to

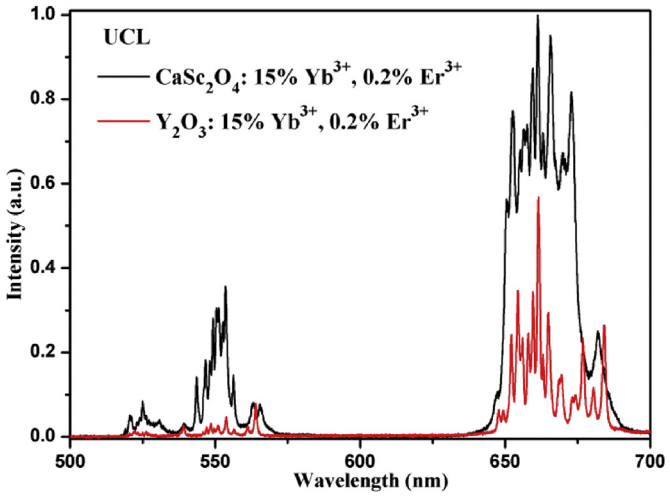

Fig. 10. UCL spectra of $CaSc_2O_4$: 15% Yb^{3+}, 0.2% Er^{3+} and Y_2O_3: 15% Yb^{3+}, 0.2% Er^{3+} under 980 nm excitation.

the similar number of dopants per-volume, being convenient for UCL intensity comparison. From Fig. 10, the area emission intensity for $CaSc_2O_4$ is observed to be 4 times as that for Y_2O_3. One of the reasons for this result can be attributed to the long lifetime of the red emitting level of Er^{3+} (I) in $CaSc_2O$. Another reason is perhaps that the absorption cross section of Yb^{3+} in $CaSc_2O_4$ is larger than in Y_2O_3 [9].

4. Conclusions

In conclusion, we have prepared $CaSc_2O_4$: Er^{3+}, xYb^{3+} upconverting phosphor by a conventional high temperature solid-state reaction. By compared the PL spectra of Er^{3+}(I) and Er^{3+}(II) on increasing Yb^{3+} concentration, two luminescent centers Er^{3+}(I) and Er^{3+}(II) are observed, which substitute for Ca^{2+} site and Sc^{3+} site, respectively. The Er^{3+}(I) centers make the main contribution to the UCL in the range of Yb^{3+} concentration of this work attributed to efficient emissions of the Er^{3+}(I) centers for the long lifetimes of Er^{3+}(I) both on the green and red emitting levels. Moreover, upconversion luminescence in $CaSc_2O_4$: 0.2% Er^{3+}, 15% Yb^{3+} is 4 times as strong as that in Y_2O_3: 0.2% Er^{3+}, 15% Yb^{3+}.

Acknowledgements

This work was partially supported by the National Key R&D Program of China (Grant No. 2016YFB0701003, 2016YFB0400605), National Natural Science Foundation of China (Grant No. 61275055, 11274007, 51402284 and 11604330) and the Natural Science Foundation of Jilin Province (Grant No. 20140101169JC, 20150520022JH and 20160520171JH).

References

[1] W.P. Qin, Z.Y. Liu, C.N. Sin, C.F. Wu, G.S. Qin, Z. Chen, K.Z. Zheng, Multi-ion cooperative processes in Yb^{3+} clusters, Light Sci. Appl. 3 (2014) e193.
[2] D. Wu, Z. Hao, W. Xiao, X. Zhang, G.H. Pan, L. Zhang, Y. Luo, L. Zhang, H. Zhao, J. Zhang, The dominant role of excitation diffusion in energy transfer upconversion of Lu_2O_3: Tm^{3+}, Yb^{3+}, J. Alloys Compd. 704 (2017) 206–211.
[3] M. Azam, V.K. Rai, Ho^{3+}-Yb^{3+} codoped tellurite based glasses in visible lasers and optical devices: Judd-Ofelt analysis and frequency upconversion, Solid State Sci. 66 (2017) 7–15.
[4] Y. Gao, Y. Hu, P. Ren, D. Zhou, J. Qiu, Effect of Li^{+} ions on the enhancement upconversion and stokes emission of $NaYF_4$:Tb, Yb co-doped in glass-ceramics, J. Alloys Compd. 667 (2016), 397–301.
[5] X. Li, Z. Xue, H. Liu, Hydro-thermal synthesis of PEGylated Mn^{2+} dopant controlled $NaYF_4$: Yb/Er up-conversion nano-particles for multi-color tuning, J. Alloys Compd. 681 (2016) 379–383.
[6] A. Dubey, A.K. Soni, A. Kumari, R. Dey, V.K. Rai, Enhanced green upconversion emission in $NaYF_4$:Er^{3+}/Yb^{3+}/Li^{+} phosphors for optical thermometry, J. Alloys Compd. 693 (2017) 194–200.
[7] S. Zeng, Z. Yi, W. Lu, C. Qian, H. Wang, L. Rao, T. Zeng, H. Liu, H. Liu, B. Fei, J. Hao, Simultaneous realization of phase/size manipulation, upconversion luminescence enhancement, and blood vessel imaging in multifunctional nanoprobes through transition metal Mn^{2+} doping, Adv. Funct. Mater. 24 (2014) 4051–4059.
[8] X. Ye, Y. Luo, S. Liu, D. Hou, W. You, Intense and color-tunable upconversion luminescence of Er^{3+} doped and Er^{3+}/Yb^{3+} co-doped $Ba_3Lu_4O_9$ phosphors, J. Alloys Compd. 701 (2017) 806–815.
[9] J. Li, J. Zhang, Z. Hao, X. Zhang, J. Zhao, Y. Luo, Intense upconversion luminescence and origin study in Tm^{3+}/Yb^{3+} codoped calcium scandate, Appl. Phys. Lett. 101 (2012) 121905.
[10] J. Li, J. Zhang, Z. Hao, L. Chen, X. Zhang, Y. Luo, Intense upconversion luminescence of $CaSc_2O_4$: Ho^{3+}/Yb^{3+} from large absorption cross section and energy-transfer rate of Yb^{3+}, ChemPhysChem 16 (2015) 1366–1369.
[11] J. Li, J. Zhang, Z. Hao, X. Zhang, J. Zhao, Y. Luo, Spectroscopic properties and upconversion studies in Ho^{3+}/Yb^{3+} Co-doped calcium scandate with spectrally pure green emission, ChemPhysChem 14 (2013) 4114–4120.
[12] J. Li, J. Zhang, Z. Hao, X. Zhang, J. Zhao, S. Lü, Y. Luo, Synthesis, morphology, and upconversion luminescence of Tm^{3+}/Yb^{3+} codoped bulk and submicro-rod $CaSc_2O_4$ phosphors, Inorg. Chem. Commun. 38 (2013) 119–122.
[13] J. Li, J. Zhang, Z. Hao, X. Zhang, J. Zhao, Y. Luo, Upconversion properties and dynamics study in Tm^{3+} and Yb^{3+} codoped $CaSc_2O_4$ oxide material, J. Appl. Phys. 113 (2013) 223507.
[14] W. Peng, S. Zou, G. Liu, Q. Xiao, J. Meng, R. Zhang, Combustion synthesis and upconversion luminescence of $CaSc_2O_4$: Yb^{3+}, Er^{3+} nanopowders, J. Rare Earth 29 (2011) 330.
[15] A. Ştefan, O. Toma, Ş. Georgescu, Upconversion luminescence in $CaSc_2O_4$ doped with Er^{3+} and Yb^{3+}, J. Lumin. 180 (2016) 376–383.
[16] Ş. Georgescu, A. Ştefan, O. Tomaa, Judd–Ofelt and energy-transfer analysis of Er^{3+} doped in $CaSc_2O_4$ ceramic samples, J. Lumin. 167 (2015) 186–192.
[17] R.D. Shannon, Revised effective ionic radii and systematic studies of interatomie distances in halides and chaleogenides, Acta Cryst. 32 (1976) 751.
[18] Z. Hao, J. Zhang, X. Zhang, X. Wang, $CaSc_2O_4$: Eu^{3+}: a tunable full-color emitting phosphor for white light emitting diodes, Opt. Mater. 33 (2011) 355–358.
[19] J. Zhang, Z. Hao, J. Li, X. Zhang, Y. Luo, G. Pan, Observation of efficient population of the red-emitting state from the green state by non-multiphonon relaxation in the Er^{3+}-Yb^{3+} system, Light Sci. Appl. 4 (2015) e239.
[20] G. Lakshminarayana, J. Qiu, M.G. Brik, G.A. Kumar, I.V. Kityk, Spectral analysis of Er^{3+}-, Er^{3+}/Yb^{3+}- and Er^{3+}/Tm^{3+}/Yb^{3+}- doped TeO_2–ZnO–WO_3–TiO_2–Na_2O glasses, J. Phys. Condens. Matter 20 (2008) 375101.
[21] H. Kuroda, S. Shionoya, T. Kushida, Mechanism and controlling factors of infrared to visible conversion process in Er^{3+} and Yb^{3+} doped phosphors, J. Phys. Soc. Jpn. 33 (1972) 125–141.